Journal of Materials Chemistry C

Accepted Manuscript

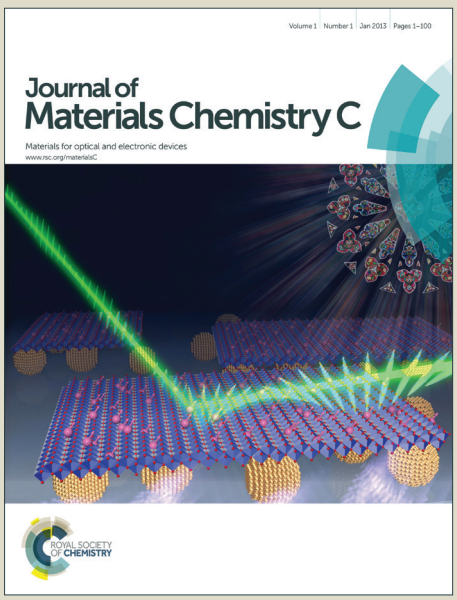

ROYAL SOCIETY OF CHEMISTRY

www.rsc.org/materialsC

Journal of
Materials Chemistry C

PAPER

High-performance light-emitting diodes using hierarchically *m*-plane GaN nano-prism light extractors†

Received 00th January 20xx,
Accepted 00th January 20xx

DOI: 10.1039/x0xx00000x

www.rsc.org/

M. Siva Pratap Reddy, Herie Park, Se-Min Kim, Seon-Ho Jang and Ja-Soon Jang*

We demonstrated the high-performance GaN-based light-emitting diodes (LEDs) with hierarchically *m*-plane nano-prism light extractors on the *n*-GaN mesa sidewalls by using a tetramethylammonium hydroxide (TMAH)-based crystallographic etching. The crystallographic etching yields to the chemically stable formation of the hierarchically *m*-plane nano-prism structures as a light extractor, the increased *p*-carriers near *p*-GaN surface, and the effective removal of native oxides on the *p*-GaN surface. These results lead to the considerable improvement of *p*-ohmic contact properties between *p*-GaN layer and ITO electrode, remarkable device-performance characteristics, improved efficiency droop, and longer device lifetime. Based on device-performance and *p*-ohmic contact data, the hierarchically *m*-plane nano-prism structure acts as a multifunctional factor having high-efficiency photon-extraction, strong packaing effect, strong suppression of leakage current along the sidewalls from *p*-GaN to *n*-GaN, and/or somewhat releasing of piezoelectric field across the quantum well region.

1. Introduction

High-performance GaN-based light-emitting diodes (LEDs) having high external quantum efficiency (EQE) and longer lifetime have been technologically issued as their lighting application areas become wider and wider from just low-current operational back light unit for mobile phones to high-current operational light-sources such as automotive lightings and large-scaled lightings.[1-5] Regarding how to enhance the EQE, there are three fundamental concepts: (i) increase of photon-escape angle and effectively escaping area,[6,7] (ii) reduction in series resistance,[8,9] and (iii) highly transparent or highly reflective electrodes with lower contact resistance.[10,11] For the photon-escape angle and escaping area in GaN-based LEDs, roughening techniques based on chemical etching have been extensively investigated because the roughen surface is very effective to satisfy them. As for the series resistance (R_s), this is very critical when we consider the EQE relation [$=(P_0/h\nu)=P_0/IV$ where P_0 is the output power, h Planck constant, ν the frequency, I the current, and V the voltage]. The reduction of the operating voltage is attainable by lowering the R_s. For the transparent or reflective conducting electrodes, lower contact resistance (between electrodes and *p*-GaN layers) as well as high-performance optical properties (such as light transmittance or light reflectance) is technologically inevitable. An increased carrier density near *p*-GaN surface is effective in reducing the contact resistance. Therefore, the requirements mentioned at least above should be satisfactory in order to enhance the EQE in GaN-based LEDs. At the same time, the LEDs should have longer life time, which is one of representative reliability issues. Very interestingly, this issue could be closely associated with the requirements above. From a standpoint of these issues, we can conclude that every technical approach should be required to verify the effectiveness between EQE and life time and show how the approaches are feasible for manufacturability.

Basically, an anisotropic mesa etching for electrical separation between *n*- and *p*-electrode is an essential step for fabricating a GaN-based LED on an electrically insulating sapphire. An inductively coupled plasma (ICP) has been widely employed to form the mesa structure because of the uniform plasma density, high etch rate, and lower plasma damage. As a result of the ICP etching, GaN crystal bonds could be physically broken at the mesa sidewalls, which can be a direct reason for high surface leakage current through the mesa sidewall surfaces. The increased surface leakage current can cause lower carrier injection toward active layers in the LEDs and hence give rise to lower EQE and higher R_s.[8,12] Due to these problems, a new approach as a second step should be introduced to recover the atomically broken crystal bonds and thus reach both electronic and structural stabilization. From this view point, a chemically we etching could be a good solution.[13,14]

Wet etching techniques have been also used to form rough surfaces of GaN-based epitaxial layers for achieving high photon-extraction from the LEDs. The rough surface can shorten a photon path and increase photon-scattering probability effectively, which can consequently lead to the overall enhancement of photon emission from the LEDs.[15,16] In particular, potassium hydroxide (KOH)-based wet etchings were effective to form crystallographic-

Department of Electronic Engineering, LED-IT Fusion Technology and Research Center (LIFTRC), Yeungnam University, Gyeongbuk 712-749, Republic of Korea. E-mail: jsjang@ynu.ac.kr; Fax: +82 53 810 7770; Tel: +82 53 810 3529
†Electronic Supplementary Information (ESI) available: See DOI: 10.1039/x0xx00000x

etched rough structures like cone-like or pyramid-like shapes in N-face GaN (grown on *c*-plane sapphire) or non-polar/semi-polar GaN surfaces.[14,17,18] In these cases, KOH serves as a catalyst and solvent for the created Ga_2O_3. The negatively charged hydroxide ions (OH^-) from KOH are quite sensitive to the electrical polarity of the GaN surface, which can be clear reasons why crystallographic etchings happen on the non-polar, semi-polar, and N-face GaN surfaces not on Ga-face GaN ones because N-face, semi-polar, and non-polar surfaces (unlike the electrically-negative-charged Ga-face surfaces) are little negative-charged.[19,20] That is, lower repulsion force on the little negative-charged surfaces can make the OH^- access the GaN, and hence the etching process can begin.

However, regarding the technical difficulty of KOH wet etching, there are representatively several difficulties as below. The first is that obtaining the optimized chemical condition is very difficult due to low volume fraction of K^+ and little blocking effect of organic molecule per ions.[21-22] In other words, achieving uniform etched shapes in whole wafers is not easy, which is believed to be one of major problems related with KOH crystallographic etching in GaN-based devices. As a second difficulty, preventing from the occurrence of unwanted defects like etch pits even at lower temperature is also difficult.[23-24] Jung et al.,[23] reporting the KOH chemical etching of GaN films on a hotplate at 100 °C for 20 min, showed triangular etch pits on the *m*-plane surface. Similar behaviours was also reported by Rass et al.[24] Once the pits are formed on the etched device, they give rise to an increased leakage current and consequently a poor device-reliability behaviour. The third is that KOH solution has a toxic nature and thus more wastewater is required to make it clean. That is, the wastewater is hazardous to the environment, indicating that the KOH etching is not environmental-friendly. On the other hand, tetramethylammonium hydroxide (mixed with H_2O solution) etching could provide a precise control of the OH^- and $(CH_3)_4N^+$, and be consequently able to give more chemically stabilized etching process.[21] The chemical reaction between TMAH and H_2O is defined as "$(CH_3)_4NOH + H_2O \rightarrow (CH_3)_4N^+ + OH^- + H_2O$". In addition, the TMAH etching is very effective to remove a native oxide on GaN surfaces, which is an important factor that can develop metal-semiconductor contact devices.[25-27] In this work, we propose a TMAH crystallographic etching technique in LED fabrication as a very fruitful and cost-innovated methodology, and also demonstrate high-performance and highly reliable LEDs with hierarchically *m*-plane nano-prism light extractors made by the proposed crystallographic etching. It is shown that the TMAH etching leads to the chemically stable formation of hierarchically *m*-plane nano-prism structures on *n*-GaN mesa sidewalls and the proposed LEDs show superior device-performance and excellent device-reliability characteristics compared to normal LEDs.

2. Experimental

2.1 LED chip fabrication

GaN-based LEDs were grown on *c*-plane sapphire substrates by using a metal-organic chemical vapor deposition (MOCVD). The LED structures are composed of a 2-μm-thick unintentionally doped GaN layer, a 2.5-μm-thick *n*-type GaN layer, InGaN/GaN multi-quantum-wells (MQWs) active layers consisting of five periods, a 0.1-μm-thick *p*-AlGaN as an electron blocking layer, and 0.12 μm-thick *p*-GaN layer. The device patterns were made by a photolithographic technique and the device area was 550×550 μm^2. ICP was employed to form a mesa structure. The TMAH:H_2O (1:3) solution was employed to perform the crystallographic etching. As soon as the mesa etching was finished, the samples were dipped into the boiling TMAH solution 85 °C for 10 min. Using a DC and RF magnetron sputtering, a 140-nm-thick indium-tin-oxide (ITO) as a transparent conducting electrode was deposited on the *p*-GaN surface and then was rapid-thermal-annealed in flowing a N_2 atmosphere at 550 °C for 1 min for achieving ohmic contacts. The Cr/Al/Ni/Au (3/250/100/300 nm) metallization scheme as a bonding-pad electrode was deposited on the *n*-GaN surface and *p*-GaN surface underneath the ITO through-hole by using electron-beam evaporation. In this work, we fabricated two types of LEDs, i.e., (i) normal LED and (ii) LEDs with hierarchically *m*-plane nano-prism structures. For simplicity, the LED with the hierarchically *m*-plane nano-prism structures is named as an *m*-plane nano-prism LED.

2.2 Post processing and packaging

After the LED fabrication, the sapphire substrates of the LED wafers were grinded up to ~110 μm by using a semi-auto wafer thinning machine (GH180-P-V, Nanosurface) and subsequently smooth wafers were made by using a single-side lapping machine (SL460PF, Nanosurface). The smooth wafers were then scribed by laser scribing machine (WLESS-600) and then were individually separated by using a semi-automatic breaker machine (NBK-107, Nano Tech). To proceed LED packaging, we used an Ag-plated Cu cup and then LED chip was physically bonded on the Cu cup by using an Ag paste. Au wires were electrically connected with *p* and *n* bonding-pad electrode of the LED chip. Finally, encapsulation process was performed using a Si resin.

2.3 Characterization techniques

Surface morphology was observed by using an atomic force microscopy (AFM). X-ray photoelectron spectroscopy (XPS, ThermoFisher Scientific, K-Alpha) measurements were performed under ultrahigh vacuum of ~5×10^{-9} Torr. Using Al Kα radiation (1486.6 eV), the XPS analysis were conducted to examine the surface characteristics of *p*-GaN surfaces before and after the TMAH etching. The mesa sidewalls were observed by using a field-emission scanning electron microscopy (FESEM, Hitachi S-4800). Photoluminescence characteristics were investigated by means of He-Cd laser (325 nm) at the power of 20 mW. The current-voltage (*I-V*), current-voltage-temperature (*I-V-T*), and output power were examined by wafer level LED measurement system (OPI-160) consisting of semiconductor parameter analyzer, optical power sensor, and temperature-adjustable chuck. The angular photon-distribution characteristics were measured by a goniometer.

3. Results and discussion

Fig. 1 shows graphically schematic illustrations for how to form *m*-plane nano-prism structures on the mesa side walls of GaN-based LEDs during the TMAH crystallographic etching process. Fig. 1a shows the *m*- and *c*-plane of hexagonal GaN structure, and Fig. 1b

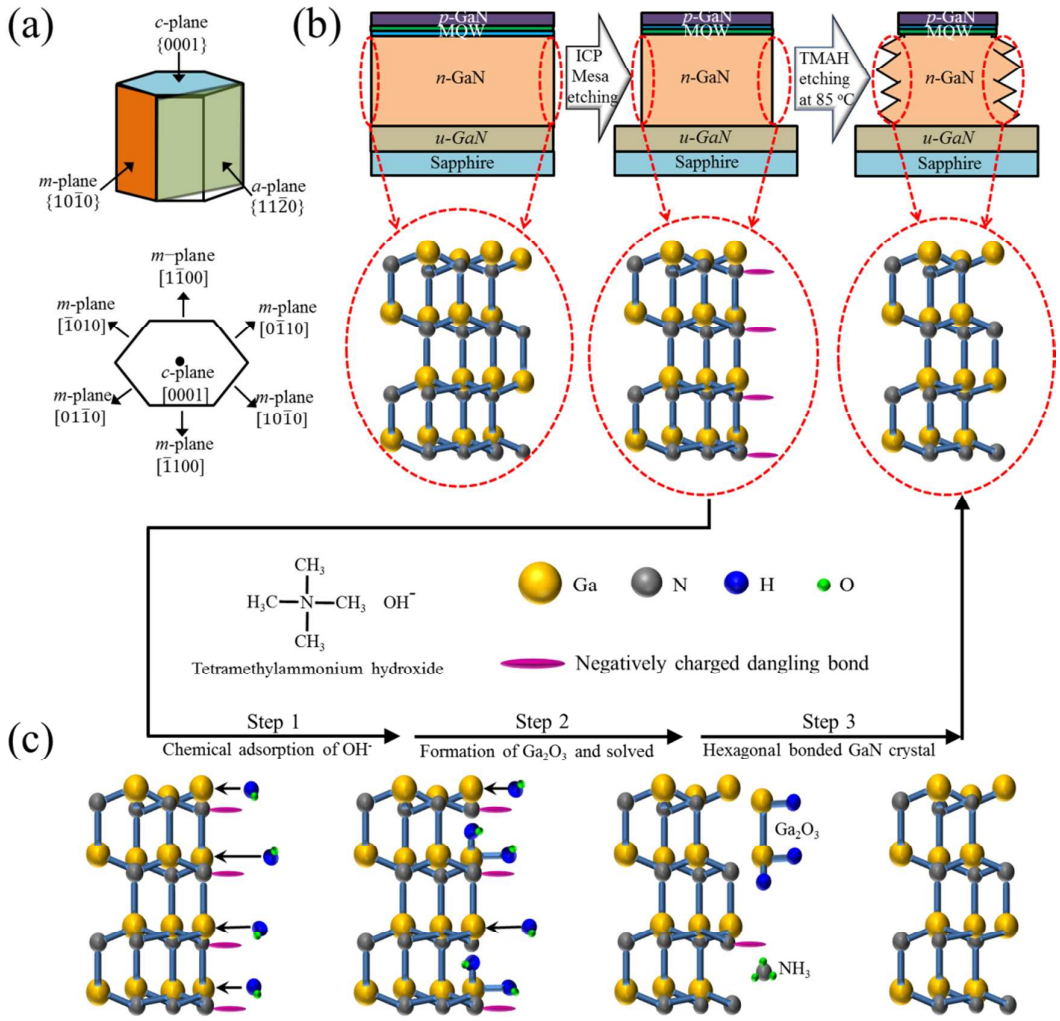

Fig. 1 (a) Hexagonal structure of *c*-plane GaN with *m*-planes (b) Graphically schematic illustrations for the steps from GaN-based LED structures before ICP mesa etching to hierarchically *m*-plane nano-prism structures of GaN mesa sidewalls after the ICP and subsequently TMAH-etching. (c) Graphically schematic descriptions for the steps of the TMAH crystallographic etching to determine the device-performance.

shows the processing steps and the corresponding crystal structures from the wurtzite Ga-face (0001) GaN before and after the ICP mesa etching to form *m*-plane nano-prisms on the mesa sidewalls after the TMAH etching. Basically, after the mesa etching of Ga-faced GaN-based epitaxial layers grown on *c*-plane sapphire substrate, an open-structured *m*-plane GaN facet is left as shown in Fig. 1b. During the TMAH etching after the mesa etching, therefore, *m*-plane GaN sidewall surfaces are chemically etched but other surfaces like *p*-GaN surface remain unchangeable. Fig. 1c illustrates how to form the *m*-plane nano-prisms on the mesa sidewalls. The dissolved hydroxide ions (OH^-) are easily adsorbed on the Ga atoms of the etched mesa side-walls, and hence Ga_2O_3.[14,19,20] The negatively charged dangling bonds attract the N atoms at the same time, and thus the N-dangling bonds are formed. The Ga_2O_3 is solved in alkali and the remaining three hydrogen atoms bond nitrogen to be NH_3 that is solved in water. During the iteration of these steps, the hierarchically *m*-plane nano-prism structures are formed on the mesa sidewalls of *n*-GaN.

Fig. 2 shows the FESEM images for the *m*-plane nano-prism structures (on the mesa sidewalls) with different image resolutions. The hierarchically trigonal structures with (10$\bar{1}$0) and (1$\bar{1}$00) *m*-planes are clearly verified to be formed on the mesa sidewalls of *n*-GaN as shown in Fig. 2b-c. However, there are no *m*-plane nano-prisms on the mesa sidewalls of the *p*-GaN and InGaN-GaN MQWs. These results may be fundamentally attributed to highly negative-charged *p*-GaN and electrically neutral MQWs. It is obviously noted that the TMAH etching is quite effective in forming the hierarchically *m*-plane nano-prism structures on the mesa sidewalls of *n*-GaN, and is also chemically stable.

In addition to the formation of the hierarchically *m*-plane nano-prism structures, an atomically feasible chemical reaction on the *p*-GaN surface in GaN-based LEDs is one of key issues that can

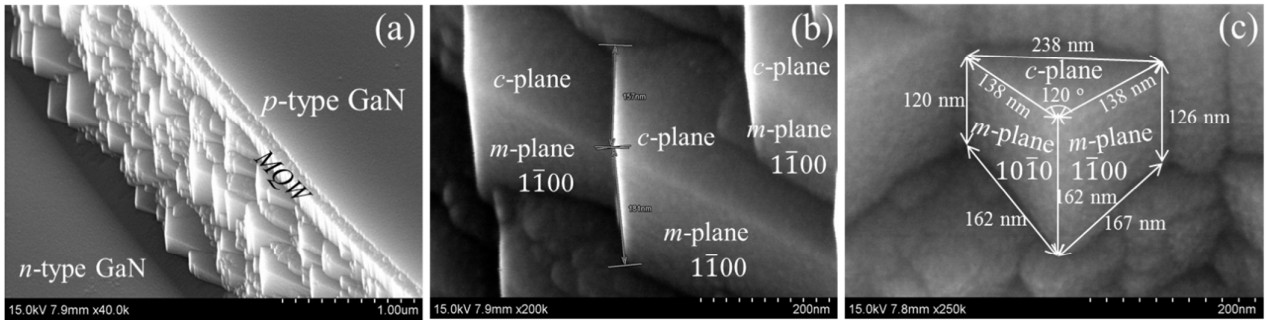

Fig. 2 (a-b) Bird's eye-view FESEM images for the hierarchically *m*-plane nano-prism structures of TMAH-LEDs under different magnifications (from 200 nm to 1 μm). (c) front-view image of the magnified *m*-plane nano-prism structure (200 nm).

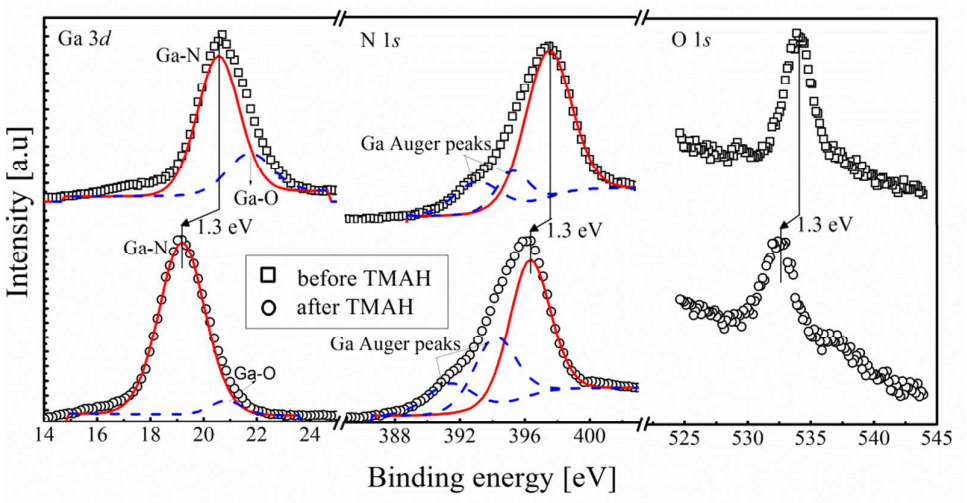

Fig. 3 XPS spectra of Ga 3*d*, N 1*s*, and O 1*s* core levels for *p*-GaN surfaces before and after the TMAH etching. Red lines are main peaks for Ga-N chemical bonding, and blue dash lines are Ga-O bonding and Ga Auger peaks in Ga 3*d* and N 1*s* spectra, respectively.

determine the device-performance properties. In fact, a major portion of whole area of GaN-based LEDs on sapphire is a *p*-GaN region. Thus, we investigated the influence of the TMAH etching on the *p*-GaN surface by using a XPS analysis. For the mesa etched *n*-GaN surface, we had already confirmed that the TMAH treatment is very effective to remove native oxide on *n*-GaN surfaces,[26,27] which is quite essential to form low-resistance ohmic contacts to *p*-GaN. Fig. 3 exhibits the core-level peaks of Ga 3*d*, N 1*s*, and O 1*s* in the *p*-GaN surface before and after the TMAH etching. The peaks of Ga 3*d* and N 1*s* core levels (after the TMAH etching) move toward lower binding energy side by 1.3 eV, indicating that the energy upward band bending of E_F-E_V becomes considerably decreased through the upward shift of valence band and consequently lowering of the energy barrier of the contact.[28] These results are clearly confirmed by the atomic composition ratio of Ga/N. The ratio of 0.79±0.1 after the TMAH etching is much lower than unit value of the ratio before the etching, which indicates increased Ga vacancies from *p*-GaN. When we consider that fact that the Ga vacancies act as an acceptor in *p*-GaN layers[29] and the increased acceptor concentration leads to the upward shift of valence band,[30] the movement of Ga 3*d* and N 1*s* peaks are consistent with the Ga/N ratio. Therefore, the TMAH etching plays an important role in increasing an acceptor near the *p*-GaN surface. Besides, the intensities of the O 1*s* peak and Ga-O bonding peak after the TMAH etching are significantly reduced in comparison with those before the etching, indicating an effective removal of the *p*-GaN surface oxide, closely similar with that of *n*-GaN surface.[26,27]

The TMAH crystallographic etching also increases the photoluminescence (PL) intensity. Fig. 4 shows the PL characteristics for the normal and *m*-plane nano-prism LED epitaxial layers. The PL intensity from the *m*-palne nano-prism LED is considerably increased by 21 % as compared to that from the normal LED. In addition, there are slightly some blue shifts of PL peaks for the *m*-plane nano-prism LED as shown in Fig. 4. These behaviors means that piezoelectric filed across the active quantum wells could be somewhat reduced as result of the formation of the hierarchically *m*-plane nano-prism as compared to the normal LED. It is noted that the increased PL intensity and blue shift are responsible for the

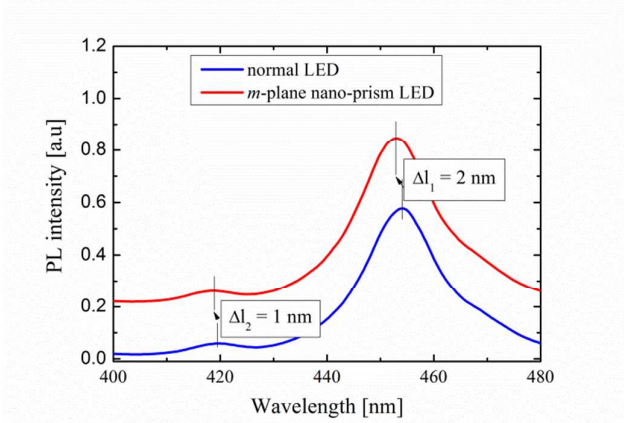

Fig. 4 Photoluminescence characteristics of the normal and *m*-plane nano-prism LED. Blue shifts for LEDs having *m*-plane nano-prism structures are observed, suggesting somewhat realizing of piezoelectric field across the quantum well region.

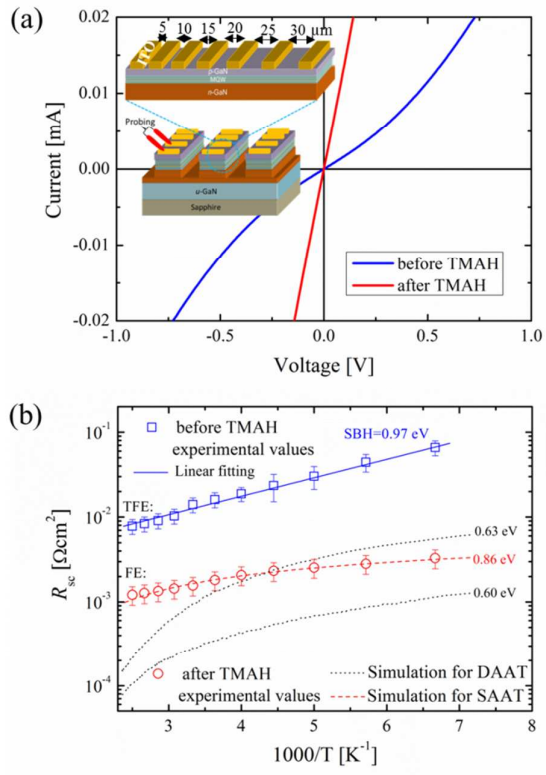

Fig. 5 (a) *I-V* characteristics of the TLM-patterned *p*-GaN of the whole LED epitaxial layers before and after the TMAH etching. Schematic descriptions of the full epi TLM patterns are shown in the inset. (b) Plots of the theoretical and experimental results of R_{sc} as a function of 1/T. the dotted and solid lines indicate the theoretical values. The TLM-patterned contact before and the TMAH etching show the TFE conduction is dominant where the contact after the etching shows the FE conduction. For all cases, shallow-acceptor-assisted tunneling (SAAT) is a main conduction instead of the deep-acceptor-assisted-tunneling (DAAT), as illustrated in Fig. S1 and the relations of S1-S3. The reduced Schottky barrier height is attributed to the decrease in the energy bandgap difference through the blue shift of surface Fermi level.

distinct contribution of the hierarchically *m*-plane nano-prisms. Additionally, the improved *p*-GaN surface from Fig. 3 may lead to the increased PL intensity owing to much faster recombination rate by means of the increased holes flowing into the active region.[31-33]

Based on the XPS results Fig. 5, the increased carriers near the *p*-GaN surface after the TMAH etching should contribute to electrical improvement of ohmic contact between *p*-GaN and ITO transparent electrode. In order to confirm the expectation, transmission line model (TLM)-patterned *p*-GaN contacts before and after the TMAH etching were fabricated. Fig. 5a illustrates the current-voltage (*I-V*) characteristics for both TLM-patterned samples. Unlike *I-V* curve of the normal *p*-GaN contact (before the TMAH etching), that of the TMAH-etched *p*-GaN contact becomes completely linear, indicating the formation of high-quality ohmic contacts. Specific contact resistance (R_{sc}) and sheet resistance (R_{sh}) of the *p*-GaN were determined from a linear fitting regression[28] among the measured resistances obtained from various TLM spacings from 5 μm to 30 μm, as shown in inset of Fig. 5a. The R_{sc} and R_{sh} of the normal contact were obtained to be 1.42×10^{-2} Ωcm^2 and 24.1 kΩ/sq, while those of the TMAH-etched contact were 1.56×10^{-3} Ωcm^2 and 8.9 kΩ/sq. It is noted that the TMAH etching results in the considerable reduction of the R_{sh}, indicating the increased carrier density near the *p*-GaN surface as expected from XPS results. The increased carriers lead to the improvement of the overall ohmic contact properties. In order to search for the TMAH-etching influence on carrier transport at the interface between ITO and *p*-GaN, the temperature-dependent R_{sc} characteristics were examined using theoretical relations of thermionic field emission (TFE) and field emission (FE) (see ESI, † Fig. S1) that are subjected to deep acceptor or shallow acceptor as described in Fig. S1. Fig. 4b shows the theoretical and experimental values of R_{sc} as a function of 1/*T*. From the comparisons, SAAT model for the both contacts is confirmed to be valid. The normal *p*-GaN shows the TFE conduction while the TMAH-etched contact exhibits the FE conduction. These different characteristics indicate that (during the TMAH etching) the *p*-GaN surface does not suffer from any occurrence of deep-level defects, and experience the increased carrier. In addition, after the TMAH etching, we did not find any morphological change on the *p*-GaN surface from atomic force microscopy analysis (see ESI, † Fig. S2). In other words, the TMAH solution is chemically stable in *p*-GaN surface and also provides usefully functional advantages as described from Figs. of 3-5.

Electrical and optical data were obtained from the packed LEDs, and the packing effect on the output power characteristics was also investigated. Fig. 6 shows the device-performance characteristics for the normal and *m*-plane nano-prism LEDs. The operating voltage (at 60 mA) and the series resistance (R_s) of the normal LED are 3.7 V and 12.5 Ω, while those of the *m*-plane nano-prism LEDs are 3.3 V and 6.2 Ω shown in Fig. 6a. The R_s was calculated by the relation of $I(dV/dI)=IR_s+nkT/q$ where *n* is ideality factor and *k* Boltzmann constant.[8,34] It is noted that the R_s of the *m*-plane nano-prism LED is roughly twice as low as that of the normal LED. The output power characteristics (as a function of the injected current) are shown in Fig. 6b. In order to investigate the packaging effect, unpackaged LEDs were compared. For the unpackaged LED, the difference of the output power between normal and *m*-plane nano-prism LED is

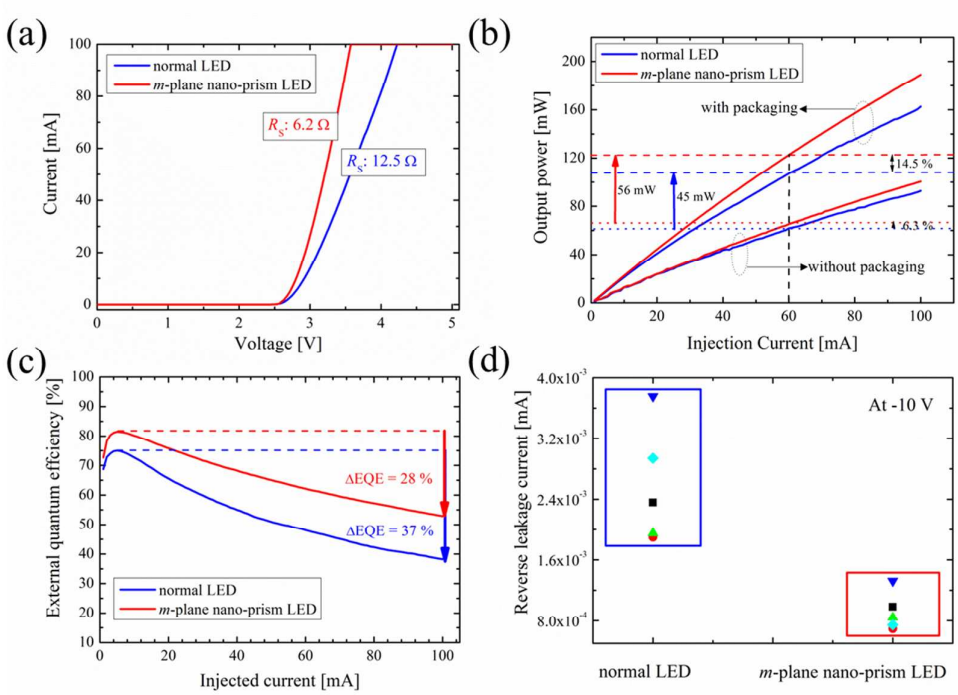

Fig. 6 Electrical and optical characteristics of the normal and *m*-plane nano-prism LEDs: (a) forward *I-V* curves, (b) optical power vs current with and without package (c) EQE vs current, and (d) plots of the reverse leakage currents at – 10 V. Note that the *m*-plane nano-prism LED shows remarkable device-performance characteristics including considerable improvement of efficiency droop at 100 mA.

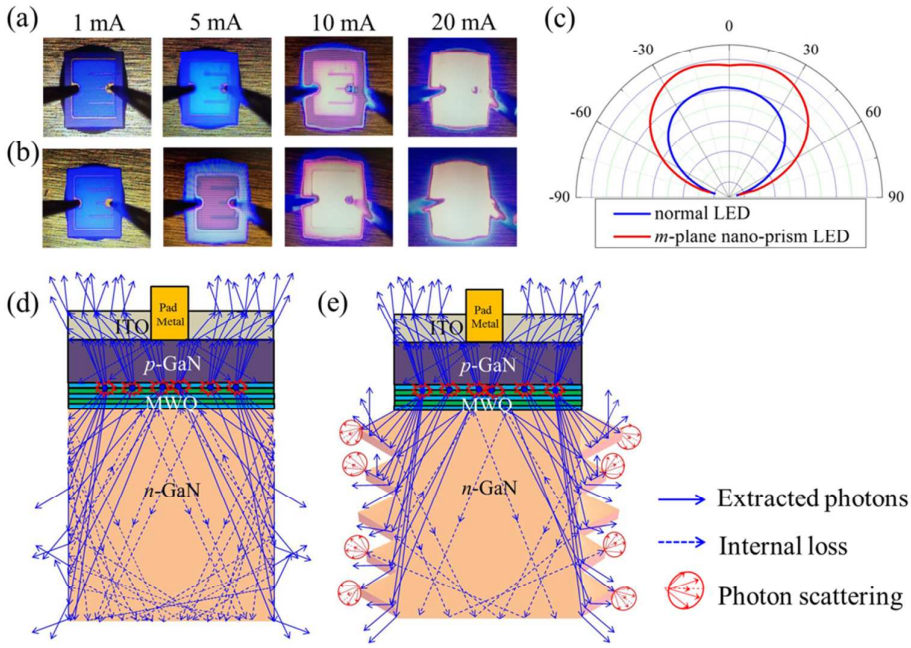

Fig. 7 Optical images for the photon emission of the (a) normal and (b) *m*-plane nano-prism LEDs as a function of the injected current. The *m*-plane nano-prism LED shows strong photon-side emission as well as strong top-emission as compared to the normal LED. (c) The near-field photon distribution characteristics of the normal and TMAH-LEDs. Schematic illustrations for feasible photon-escape paths of the (d) normal LED and (e) *m*-plane nano-prism LED. The comparison reveals that the hierarchically *m*-plane nano-prism acts as an excellent photon extractor due to wider escape angle, increased photon scattering, and reduced internal-reflection loss.

6.3 %. On the other hand, the packaged LED shows the remarkable improvement of the output power by 14.5 % as compared to the unpackaged LEDs. The output power of the normal LED is improved by 45 mW after the packaging, while that of the *m*-plane nano-prism LED is improved by 56 mW. These results indicate that the LED with hierarchically *m*-plane GaN nano-prism light extractors is much more effective in enhancing the packaging effect than the normal LED, which can be expected to be directly applicable to mass production. The electrical and optical improvement in the *m*-plane nano-prism LED eventually yields to a considerable increase of the EQE, and the efficiency droop at 100 mA is also reduced by 9 % as shown in Fig. 6c. From Fig. 6d, in addition, the reverse leakage current (at -10 V) of the *m*-plane nano-prism LED becomes obviously reduced as compared to that of the normal LED. Based on the device-performance characteristics, the significant improvement of the overall properties can be responsible for the electrically improved *p*-GaN surface, lower resistance *p*-ohmic contact, and increased photon-escape probability.

Fig. 7 illustrates the optical images depending on the injected currents, photon-emission distribution characteristics, and schematic diagrams for comparisons of feasible photon paths. From the optical images shown 7a-b, the lateral and overall photon-emission of the *m*-plane nano-prism LED is much stronger than those of the normal LED with increasing the current. In addition, the angular photon-emission distribution characteristics shown in Fig. 7c clearly show that the LED with *m*-plane nano-prism structures has wider angle and stronger intensity. Based on these characteristics, we propose the feasible photon-escape paths as displayed in Fig. 7d-e. Unlike the normal LED, the *m*-plane nano-prism LED has a lot of photon-scattering positions at the nano-prism structures, meaning that the overall internal reflection loss is dramatically decreased through the increased photon-scattering centers. Therefore, the *m*-plane nano-prism structures acts as a hierarchical light extractor for the *m*-plane nano-prism LED.

Device reliability is one of main technological issues, and thus we investigated how much the *m*-plane nano-prism LED is induced strong as compared to the normal LED. To verify the device reliability characteristics, we performed a high-stress acceleration test under the forward current of 425 mA at room temperature. Fig. 8 exhibits plots of the drop rate (P_0^{DR}) of optical power (P_0) for the normal and *m*-plane nano-prism LED as a function of stress time. P_0^{DR} can be expressed as following[8]

$$P_0^{DR} = \frac{P_0^{initial} - P_0^{initial}\exp(-\alpha t)}{P_0^{initial}} \times 100[\%] = [1-\exp(-\alpha t)].100\% \qquad (1)$$

where $P_0^{initial}$ is the initial output power measured at the current injection time of 0.1 s, α is the degradation rate, and t is the acceleration time. The α of the *m*-plane nano-prism LED is around 10 times as low as that of the normal LED, indicating that the *m*-plane nano-prism LED is much more reliable and has a longer lifetime. The enhanced reliability characteristics of the *m*-plane nano-prism LED is clearly due to the combined effects among the reduced leakage current, decreased series resistance, and somewhat released piezoelectric field. Based on the electrical, optical, and reliability characteristics, we suggested that the LED having a hierarchical nano-prism light extractor (formed from the TMAH crystallographic etching) is very promising device-structure that can provide excellent reliability characteristics and high-performance device-operating characteristics.

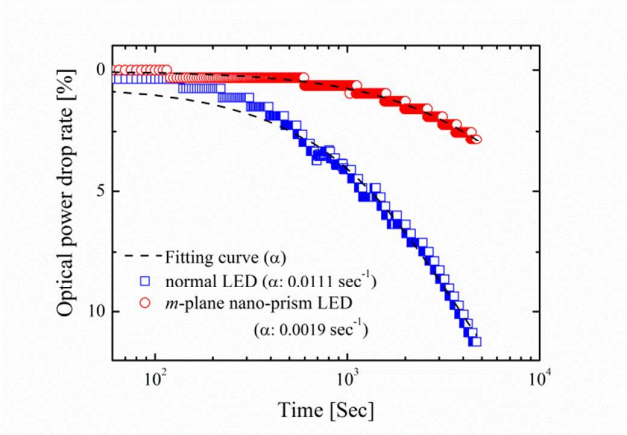

Fig. 8 Time-dependent power drops of normal and *m*-plane nano-prism LED at an injection current of 425 mA. Fitting curves are theoretical results calculated from eqn. (1).

4. Conclusions

In summary, we successfully demonstrated high-performance and highly reliable GaN-based LEDs with *m*-plane nano-prism light extractors on the mesa sidewalls by using the TMAH-based crystallographic etching. The TMAH etching leads to the chemically stable formation of *m*-plane nano-prism structures on *n*-GaN mesa sidewalls, the increased carrier density near the *p*-GaN surface, and the effective removal native oxide on the *p*-GaN surface. These outstanding advantages result in the improved *p*-ohmic contact properties between ITO electrode and *p*-GaN, considerably improved device-performance characteristics, and excellent reliability characteristics. Regarding the packaging effect, the *m*-plane nano-prism LED is much stronger than the normal LED, which is very promising for mass production. Based on various investigation results, the hierarchically *m*-plane nano-prism structures clearly act as a light extractor in GaN-based LEDs, and also play an important role in enhancing the leakage suppression and somewhat releasing piezoelectric fields across the multiple quantum well region. Thus, the LED with hierarchically *m*-plane nano-prism light extractors is a highly promising structure that can satisfy high device-performance and excellent reliability characteristics.

Acknowledgements

This study was supported by MOTIE of Korea through the industrial infrastructure program under Grant No: 10033630, and Yeungnam University Grant.

References

1 E. Matioli, S Brinkley, K. M.Kelchner, Y.-L. Hu, S. Nakamura, S. DenBaars, J. Speck and C. Wiesbuch, *Light Sci. Appl.*, 2012, **e22**, 1.
2 R.-H. Horng, K.-C. Shen, C.-Y. Yin, C.-Y. Huang and D.-S. Wuu, *Opt. Express*, 2013, **21**, 14452.
3 X. Ren, X. Zhang, N. Liu, L. Wen, L. Ding, Z. Ma, J. Li, J. Han and Y. Gao, *Adv. Funct. Mater*., 2015, **25**, 2182.
4 H. Jia, L. Guo, W. Wang and H. Chen, *Adv. Mater*., 2009, **21**, 4641.
5 S. Pimputkar, J. S. Speck, S. P. DenBaars and S. Nakamura, *Nat. Photonics*, 2009, **3**, 180.
6 Z. Yin, X. Liu, Y. Wu, X. Hao and X. Xu, *Opt. Express*, 2012, **20**, 1013.
7 E.-H. Park, J. Jang, S. Gupta, I. Ferguson, C.-H. Kim, S.-K. Jeon and J.-S. Park, *Appl. Phys. Lett.*, 2008, **93**, 191103.
8 J.-S. Jang, *Appl. Phys. Lett*., 2008, **93**, 081118.
9 J.-S. Jang, D. Kim and T.-Y. Seong, *IEEE Photon. Technol. Lett*., 2006, **18**, 1536.
10 J.-K. Kim, S. Chhajed, M. F. Schubert, E. F. Schubert, A. J. Fischer, M. H. Crawford, J. Cho, H. Kim and C. Sone, *Adv. Mater*., 2008, **20**, 801.
11 M. Oh and H. Kim, *Opt. Express*, 2013, **21**, 20857.
12 T.-X. Lee, K.-F. Gao, W.-T. Chien and C.-C. Sun, *Opt. Express*, 2007, **15**, 6670.
13 J. M. Lee, K. S. Lee and S. J. Park, *J. Vac. Sci. Technol. B*, 2004, **22**, 479.
14 S. Jung, K.-R. Song, S.-N. Lee and H. Kim, *Adv. Mater*., 2013, **25**, 4470.
15 C.-F. Lin, Z.-J. Yang, J.-H. Zheng and J.-J. Dai, *IEEE Photon. Technol. Lett*., 2005, **17**, 2038.
16 T. Fujii, Y. Gao, R. Sharma, E. L. Hu, S. P. DenBaars and S. Nakamura, *Appl. Phys. Lett*., 2004, **84**, 855.
17 Y. Jung, J. Kim, S. Jang, K.-H. Baik, Y.-G. Seo and S.-M. Hwang, *Opt. Express*, 2010, **18**, 9728.
18 K.-H. Baik, H.-Y. Song, S.-M. Hwang, Y. Jung, J. Ahn and J. Kim, *J. Electrochem. Soc.*, 2011, **158**, D196.
19 D. Li, M. Sumiya, S. Fuke, D. Yang, D. Que, Y. Suzuki and Y. Fukuda, *J. Appl. Phys*., 2001, **90**, 4219.
20 D. Zhuang and J. H. Edgar, *Mater. Sci. Eng. R*, 2005, **48**, 1.
21 I. Zubel, I. Barycka, K. Kotowska and M. Kramkowska, *Sens. Actuators A*, 2001, **87**, 163.
22 M. Shikida, K. Sato, K. Tokoro and D. Uchikawa, *Sens. Actuators A*, 2000, **80**, 179.
23 Y. Jung, K.-H. Baik, M. A. Mastro, J. K. Hite, C. R. Eddy Jr and J. Kim, *Phys. Chem. Chem. Phys*. 2014, **16**, 15780.
24 J. Rass, T. Wernicke, R. Kremzow, W. John, S. Einfeldt, P. Vogt, M. Weyers and M. Kneissl, *Phys. Status Solidi A*, 2010, **207**, 1361.
25 K.-W. Kim, S.-D. Jung, D.-S. Kim, H.-S. Kang, K.-S. Im, J.-J. Oh, J.-B. Ha, J.-K. Shin and J.-H. Lee, *IEEE Electron Device Lett*., 2001, **32**, 1376.
26 M. S. P. Reddy, D.-H. Son, J.-H. Lee, J.-S. Jang and V. R. Reddy, *Mater. Chem. Phys*., 2014, **143**, 801.
27 M. S. P. Reddy, J.-H. Lee and J.-S. Jang, *Electron. Mater. Lett*., 2014, **10**, 411.
28 J.-S. Jang, T.-Y. Seong and S.-R. Jeon, *Appl. Phys. Lett*., 2007, **91**, 092129.
29 P. Boguslawski, E. L. Briggs and J. Bernholc, *Phys. Rev. B*, 1995, **51**, 17255.
30 J.-S. Jang and T.-Y. Seong, *J. Appl. Phys*., 2000, **88**, 3064.
31 U. Kaufmann, M. Kunzer, M. Maier, H. Obloh, A. Ramakrishana, B. Santic and P. Schlotter, *App. Phys. Lett*., 1998, **72**, 1326.
32 L. S. Wang, W. K. Fong, C. Surya, K. W. Cheah, W. H. Zheng and Z. G. Wang, *Solid-State Electron*., 2001, **45**, 1153.
33 M. A. Reshchikov, J. D. McNamara, S. Fernandez-Garrido and R. Calarco, *Phys. Rev. B*., 2013, **87**, 115205.
34 D. K. Schroder, *Semiconductor Material and Device Characterization*, Wiley:Interscience, NJ, 3rd ed., 2006.

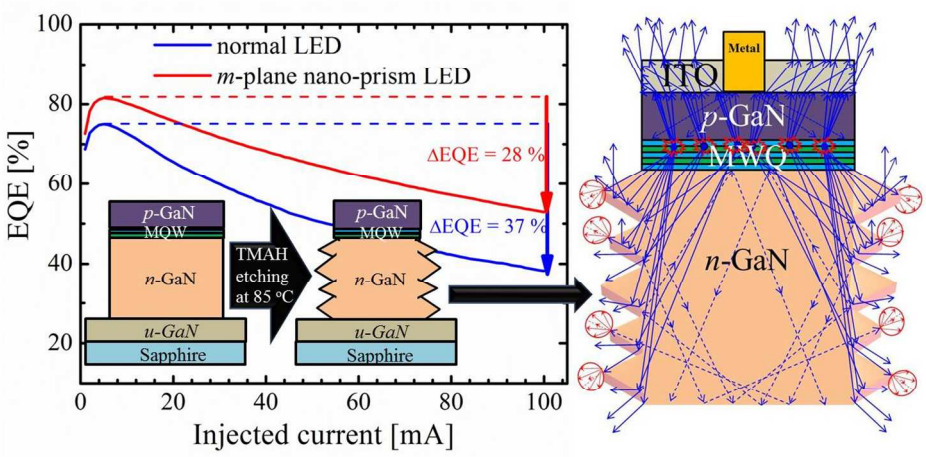

254x190mm (300 x 300 DPI)